Crystallographically oriented Zn nanocrystals formed in ZnO by Mn + -implantation

Y. J. Li, B. Zhang, W. Lu, Y. Wang, and J. Zou

Citation: Applied Physics Letters **93**, 131919 (2008); doi: 10.1063/1.2996028

View online: http://dx.doi.org/10.1063/1.2996028

View Table of Contents: http://scitation.aip.org/content/aip/journal/apl/93/13?ver=pdfcov

Published by the AIP Publishing

Crystallographically oriented Zn nanocrystals formed in ZnO by Mn^+-implantation

Y. J. Li,[1] B. Zhang,[1,a)] W. Lu,[1,b)] Y. Wang,[2] and J. Zou[2]
[1]*National Lab for Infrared Physics, Shanghai Institute of Technical Physics, Chinese Academy of Sciences, 500 Yu Tian Road, Shanghai 200083, China*
[2]*School of Engineering and Centre for Microscopy and Microanalysis, The University of Queensland, St. Lucia, Queensland 4072, Australia*

(Received 4 July 2008; accepted 16 September 2008; published online 3 October 2008)

The nanostructural characteristics of ZnO implanted with Mn^+ to doses ranging from 1×10^{15} to 1×10^{17} cm^{-2} are systematically studied for both as-implanted and postannealed cases. The detailed structural characterizations confirmed that the Mn^+ implantation and postannealing result in (1) the formation of crystallographically orientated Zn nanocrystals in the ZnO matrix and (2) Mn atoms occupy the Zn sites in ZnO. © *2008 American Institute of Physics*.
[DOI: 10.1063/1.2996028]

Recently, ZnO-based diluted magnetic semiconductors (DMSs) and their potential applications in spintronics have attracted extensive attention. The ferromagnetism of DMSs can be resulted from carrier-mediated exchange interaction in the alloyed ZnO with transition metal (TM) ions, typically in a concentration range of 1–25 at. % relative to the total number of Zn atoms.[1,2] A significant interest has been focused on the development of *p*-type $Zn_{1-x}Mn_xO$ due to their predicted room temperature ferromagnetism for future spintronics applications.[3] As a mature technique to alloy the TM ions with ZnO, the TM ions implantation has been used to create the ferromagnetism of ZnO based DMSs. However, many investigations on such DMSs systems were focused on the formations of clusters, precipitates, or secondary phases and their responsibilities in terms of the ferromagnetism. The high dose of ion implantation with Fe,[4] Co,[5,6] and Ni (Ref. 5), has created the nanocrystals (NCs) of these TMs, which may be responsible for the observed ferromagnetic properties. However, few studies have been carried out on the nanostructures induced by Mn^+ implantation in ZnO. In this letter, we comprehensively investigated the nanostructures of Mn^+ ions implanted ZnO using cross-sectional transmission electron microscopy (XTEM), X-ray diffraction (XRD), and Raman microscopy. It was revealed that implanted Mn atoms occupy the Zn site and Zn atoms are precipitated to form Zn NCs from the Mn^+ implanted ZnO matrix, which is different from those results of the Fe^+, Co^+, and Ni^+ implanted ZnO.

Hydrothermally grown single-crystal ZnO samples with (0001) orientation used in this study were purchased from MTI Company. They were nominally undoped and double-side polished. Mn^+ ions were implanted into these samples at room temperature with a dose ranging from 1×10^{15} to 1×10^{17} cm^{-2}. The energy of Mn^+-implantation was 200 keV, and the ion beam flux was $\sim2.3\times10^{13}$ cm^{-2} s^{-1}. During implantation, the samples' (0001) surface normals were tilted 7° relative to the incident beam to minimize the channeling effect. After implantation, some samples were subject to a 5 min rapid thermal annealing at 725 °C in flowing N_2 ambient.

XTEM specimens were prepared using a tripod technique, followed by a final thinning using a Gatan precision ion polishing system.[7,8] The XTEM and energy filtered TEM (EFTEM) experiments were carried out in a FEI Tecnai F30 TEM with Gatan image filter system, operating at 300 kV. XRD was carried out in a two-dimensional diffraction system (Bruker-AXS, D8 Discover with GADDS) operating with Cu $K\alpha$ radiation ($\lambda=1.5418$ Å) at 40 kV and 40 mA. Micro-Raman backscattering experiments were performed using a Jobin–Yvon LabRam-INFINITY system with the 514.53 nm line of an Ar^+ ion laser as an excitation source.

Figures 1(a)–1(d) are typical XTEM and EFTEM images of the as-implanted and the annealed ZnO with the Mn^+ implantation dose of 1×10^{17} cm^{-2}, respectively. Figures 1(b) and 1(d) reveal a two-layered structure in the annealed sample comparing with the as-implanted [Figs. 1(a) and 1(c)]. The first layer extends from the surface to a depth of ~80 nm, where ~20–50 nm diameter voids or gas bubbles[9,10] are formed, and the surface of the sample is rough. Below this layer, the underlying layer extends to a depth of ~160 nm where the corresponding EFTEM mappings [Figs. 1(d) and 1(e)] reveal the presence of ~20–25 nm diameter Zn-rich precipitates. By the EFTEM Mn elemental maps, the Mn ions implantation has the penetration depth of ~120 nm. The thermal annealing makes Mn diffuse toward to the surface and the depth of ~160 nm.[7,8] Figure 1(f) is a selected area electron diffraction (SAED) pattern, where two sets of diffraction patterns can be seen and both sets can be indexed as ZnO and Zn diffraction patterns.[11,12]

Figures 2(a) shows the θ-2θ XRD scans for the samples with the implantation dose of 1×10^{17} cm^{-2} and unimplanted ZnO. As expected, intense ZnO (0002) and (0004) peaks are observed. Careful examination of the ZnO (0002) peak shows a shoulderlike structure at $2\theta\approx36.2°$, which corresponds to the Zn (0002) peak (Zn has a hexagonal structure with $a=0.2665$ and $c=0.4947$ nm).[11] Figures 2(b) and 2(c) are ϕ scans of grazing incidence XRD (GIXRD), for the as-implanted and the annealed ZnO, respectively. The ϕ scans of NCs hexagonal Zn $\{10\bar{1}1\}$ and $\{11\bar{2}2\}$ and hexagonal ZnO $\{10\bar{1}3\}$ show a sixfold symmetry. The XRD results reveal that Zn NCs are crystallographically oriented within

a)Electronic mail: bozhang@mail.sitp.ac.cn.
b)Electronic mail: luwei@mail.sitp.ac.cn.

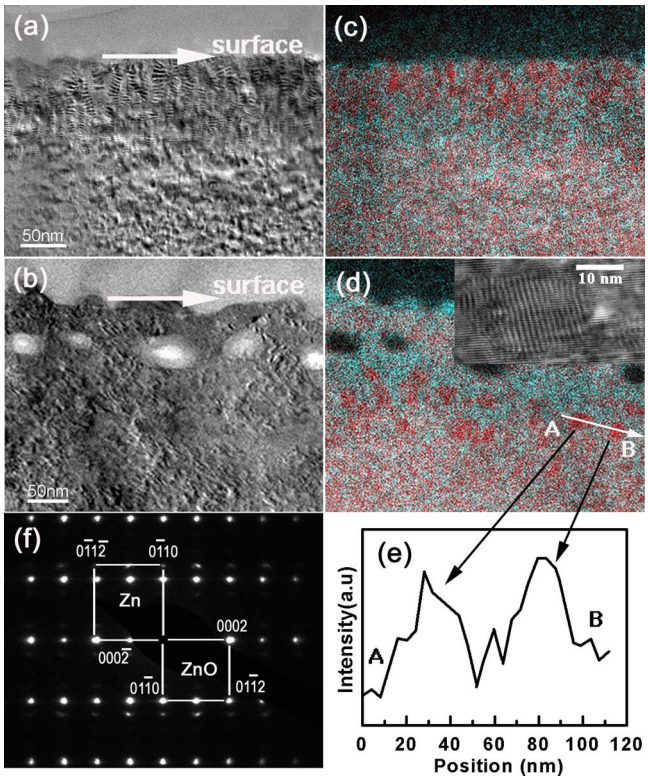

FIG. 1. (Color online) Typical XTEM images of (a) as-implanted and (b) annealed ZnO implanted with Mn^+ dose of 1×10^{17} cm^{-2}. (c) and (d) are corresponding EFTEM images of (a) and (b) with red denoting elemental Zn and light-blue representing O. (e) Intensity profile of Zn from A to B line in (d). (f) SAED patterns showing Zn and ZnO having perfect orientation relationship. The inset displays the moiré contrasts of Zn and ZnO.

the ZnO matrix. The orientation relationship is $[10\bar{1}0]_{Zn}\|[10\bar{1}0]_{ZnO}$ and $(0002)_{Zn}\|(0002)_{ZnO}$, which is consistent with the SAED result.[11,12] The nucleation sites for Zn NCs have already formed during implantation (interstitial Zn atoms induced by implantation moved and aggregated into Zn clusters energetically favorable during implantation). The comparison of the XRD patterns shows that the annealed sample has the higher XRD intensity and sharper diffraction peaks for both ZnO and Zn NCs, indicating that the annealing has recovered the crystallinity of implanted ZnO and promoted the growth of Zn NCs. The XRD and EFTEM study for other samples implanted with doses of lower than 1×10^{17} cm^{-2} (not shown here) do not yield any evidence of porosity or precipitated hexagonal Zn NCs.

Figure 3 presents the Raman spectra of unimplanted ZnO and as-implanted ZnO with different Mn^+ doses. Three normal modes at 99, 331, and 437 cm^{-1} are observed in the implanted ZnO, which can be assigned to ZnO (E_2^{low}), ($E_2^{high}-E_2^{low}$), and (E_2^{high}), respectively.[13] Apart from these normal modes of ZnO, two additional broad bands at 50–250 and 500–580 cm^{-1} together with a peak at 565 cm^{-1} can be seen when comparing with the unimplanted ZnO [Fig. 3(e)]. the intensity of three normal modes decreases but the mode at 565 cm^{-1} and the two broad bands increase with increasing the Mn^+ implantation dose [Figs. 3(a)–3(d)]. This may be due to the increased lattice damage and defects induced by the implantation with increasing the Mn^+ implantation dose.[14] It should be noted that the strong crystallinity of the ZnO matrix after the implantation is still preserved (see Figs. 3 and 2), because ZnO has very strong dynamic annealing[15]

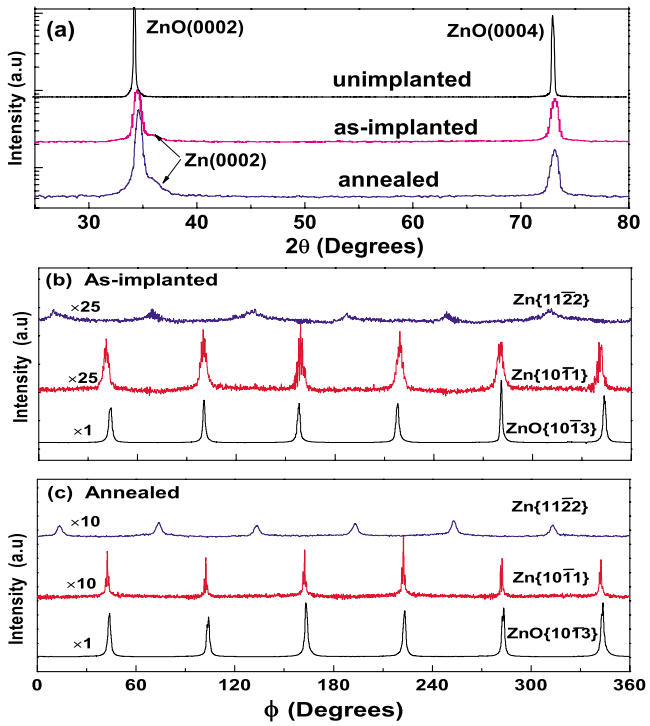

FIG. 2. (Color online) XRD patterns of the as-implanted and the annealed ZnO implanted with Mn^+ dose of 1×10^{17} cm^{-2}: (a) θ-2θ scans. [(b) and (c)] ϕ scans of GIXRD for hexagonal Zn {11$\bar{2}$2}, {10$\bar{1}$1}, and ZnO {10$\bar{1}$3}, for the as-implanted and the annealed ZnO, respectively.

Figures 4(a)–4(d) show the Raman spectra of the annealed ZnO. As can be seen when comparing with Fig. 3 (as-implanted cases), two new modes at 70 and 530 cm^{-1} appear when Mn^+ implantation dose reaches 1×10^{16} cm^{-2} [Figs. 4(a)–4(c)], respectively. These two modes increase with increasing the Mn^+ dosage. There is no peak near 70 cm^{-1} in ZnO's one-phonon density of states.[16] To understand the mode at 70 cm^{-1}, we note that E_{2g} phonon in hexagonal Zn crystal is responsible to a mode at 70 cm^{-1}.[17] To further confirm this, we collected a Raman spectrum of pure Zn [Fig. 4(e)] where a mode at 70 cm^{-1} is clearly seen. Based on these studies and the fact that pure Zn was detected by both x-ray and electron diffraction and EFTEM, we believe that the mode at 70 cm^{-1} observed in the annealed ZnO

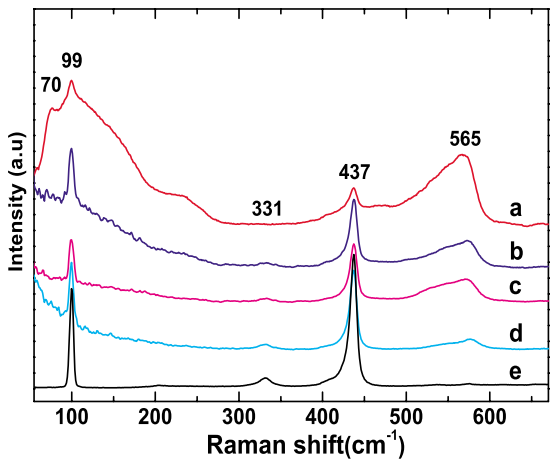

FIG. 3. (Color online) Raman spectra of the as-implanted ZnO with different Mn^+ doses: (a) 1×10^{17} cm^{-2}, (b) 5×10^{16} cm^{-2}, (c) 1×10^{16} cm^{-2}, (d) 1×10^{15} cm^{-2}, and (e) unimplanted ZnO.

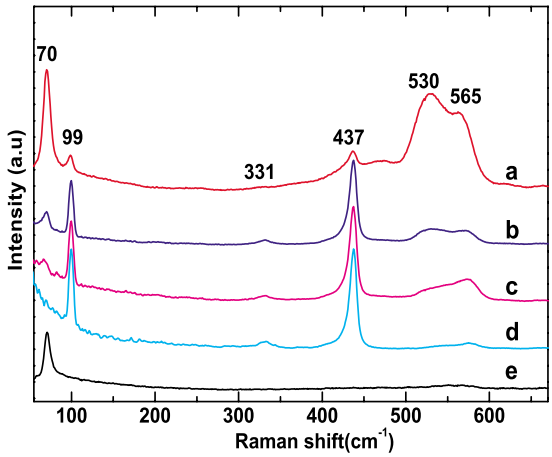

FIG. 4. (Color online) Raman spectra of the annealed ZnO implanted with different Mn^+ doses: (a) 1×10^{17} cm^{-2}, (b) 5×10^{16} cm^{-2}, (c) 1×10^{16} cm^{-2}, (d) 1×10^{15} cm^{-2}, and (e) Zn polycrystals.

[Figs. 4(a)–4(c)] and the highly Mn^+ implanted ZnO [Fig. 3(a)] must belong to Zn NCs precipitated from Mn^+ implanted ZnO. To understand the mode at 530 cm^{-1}, we also note that this mode has been confirmed as Mn occupies the Zn sites in ZnO.[14]

Careful comparison of Raman spectra between the as-implanted ZnO and the annealed ZnO shows that the two broad bands observed in the as-implanted ZnO almost disappear after the annealing. It is generally believed that the lattice damage and defects induced by the implantation are responsible for the abnormal bands in the as-implanted ZnO. As a consequence, we consider that the two broad bands are caused by the lattice damage and defects, and the annealing recover the lattice damage and, in turn, lead to the bands disappearing. It is of interest to note that the abnormal mode at 565 cm^{-1} remains after the annealing. To understand this, we note that the mode at 565 cm^{-1} has been frequently observed in ZnO nanoparticles.[18] We anticipate that the fundamental reason of the mode at 565 cm^{-1} is due to the lattice defects caused by Mn occupying the Zn sites,[14] and the formation of nanosized ZnO domains caused by the Zn precipitation from ZnO lattice during the implantation and the annealing cannot recover the loss of Zn atoms in the ZnO matrix. The Raman spectra of the annealed ZnO show that the modes at 70 and 530 cm^{-1} increase with increasing the Mn^+ dosage, suggesting that the higher the Mn^+ dosage, the more the Zn NCs and the more the Mn occupying the Zn sites in ZnO.

In conclusion, crystallographically orientated Zn NCs are formed in ZnO during Mn^+ implantation to the dose of 1×10^{17} cm^{-2}. During the postannealing, implanted Mn atoms occupy Zn sites in ZnO and Zn NCs are precipitated from matrix for implantation doses above 1×10^{16} cm^{-2}. The behaviors of abnormal modes/bands found in the Raman spectra in the as-implanted and annealed ZnO provide footprints of the structural and chemical variations of ZnO experienced with implantation and postannealing.

Chinese National Key Basic Research Special Fund (2004CB619004 and 2007CB613206) and the Australian Research Council are acknowledged for their financial support.

[1]T. Dietl, H. Ohno, F. Matsukura, J. Cibert, and D. Ferrand, Science **287**, 1019 (2000).
[2]K. Sato and H. Katayama-Yoshida, Jpn. J. Appl. Phys., Part 2 **40**, L334 (2001).
[3]S. A. Wolf, D. D. Awschalom, R. A. Buhrman, J. M. Daughton, S. V. Molnar, M. L. Roukes, A. Y. Chtchelkanova, and D. M. Treger, Science **294**, 1488 (2001).
[4]K. Potzger, S. Q. Zhou, H. Reuther, A. Mucklich, F. Eichhorn, N. Schell, W. Skorupa, M. Helm, J. Fassbender, T. Herrmannsdorfer, and T. P. Papageorgiou, Appl. Phys. Lett. **88**, 052508 (2006).
[5]S. Q. Zhou, K. Potzger, J. V. Borany, R. Grozschel, W. Skorupa, M. Helm, and J. Fassbender, Phys. Rev. B **77**, 035209 (2008).
[6]D. P. Norton, M. E. Overberg, S. J. Pearton, K. Pruessner, J. D. Budai, L. A. Boatner, M. F. Chisholm, J. S. Lee, Z. G. Khim, Y. D. Park, and R. G. Wilson, Appl. Phys. Lett. **83**, 5488 (2003).
[7]Y. Wang, J. Zou, Z. M. Zhao, X. H. Han, X. Y. Zhou, and K. L. Wang, J. Appl. Phys. **103**, 066104 (2008).
[8]Y. Wang, J. Zou, Z. M. Zhao, X. H. Han, X. Y. Zhou, and K. L. Wang, Appl. Phys. Lett. **92**, 101913 (2008).
[9]V. A. Coleman, H. H. Tan, C. Jagadish, S. O. Kucheyev, and J. Zou, Appl. Phys. Lett. **87**, 231912 (2005).
[10]S. O. Kucheyev, J. S. Williams, and C. Jagadish, Vacuum **73**, 93 (2004).
[11]Y. Ding, X. Y. Kong, and Z. L. Wang, J. Appl. Phys. **95**, 306 (2004).
[12]J. G. Wang, M. L. Tian, N. Kumar, and T. E. Mallouk, Nano Lett. **5**, 1247 (2005).
[13]R. Cusco, E. Alarcon-Llado, J. Ibanez, L. Artus, J. Jimenez, B. G. Wang, and M. J. Callahan, Phys. Rev. B **75**, 165202 (2007).
[14]S. Venkataraj, N. Ohashi, I. Sakaguchi, Y. Adachi, T. Ohgaki, H. Ryoken, and H. Haneda, J. Appl. Phys. **102**, 014905 (2007).
[15]S. O. Kucheyev, J. S. Williams, C. Jagadish, J. Zou, C. Evans, A. J. Nelson, and A. V. Hamza, Phys. Rev. B **67**, 094115 (2003).
[16]J. Serrano, A. H. Romero, F. J. Manjon, R. Lauck, M. Cardona, and A. Rubio, Phys. Rev. B **69**, 094306 (2004).
[17]H. Olijnyk, A. P. Jephcoat, D. L. Novikov, and N. E. Christensen, Phys. Rev. B **62**, 5508 (2000).
[18]Z. D. Fu, Y. S. Cui, S. Y. Zhang, J. Chen, D. P. Yu, S. L. Zhang, L. Niu, and J. Z. Jiang, Appl. Phys. Lett. **90**, 263113 (2007).